Int. J. Dyn. Fluids. Vol.1 no.1(2005), pp. 1-25

Temporal and Spatial Instabilities of the Flow in the Blood Vessels as Multi-Layered Compliant Tubes

Mahmoud HAMADICHE[1] and **Natalya KIZILOVA**[2]

[1]*Laboratoire de Mécanique des Fluides et d'Acoustique, Ecole Centrale de Lyon, 69131 Ecully CEDEX, France*

[2]*Department of Theoretical Mechanics, Kharkov National University, Svobody Sq., 4, 61195, Kharkov, Ukraine*

Abstract The stability of the Poiseuille flow of a viscous incompressible fluid in a multilayered non-isotropic viscoelastic tube is investigated. The compliant wall of the tube is allowed to be in a dynamic interaction with the flow. The material and geometrical parameters of the model correspond to mechanical properties and structure of the arterial vessels. A numerical method is developed in order to find the eigenvalues of the system in the limit of the linear stability analysis. Both temporal and spatial eigenvalues of the system are computed and compared to the eigenvalues for the isotropic wall. The multivarious effects of the anisotropy on the eigenvalues of the system are investigated. The influence of the viscosities, shear and Young's modulus of the layers on the most unstable mode is examined. In view of the importance of the result in medical diagnostics, a particular attention is paid to the speed of propagation of the most unstable mode.

1 Introduction

Mechanical factors and fluid-structure interaction define normal physiological state and function of arteries and veins. When blood moves through the vessel both hydrostatic pressure and viscous drag at the wall influence the shape and mechanical properties of the vessel wall. The stress field in the wall determines its inner structure and geometry of the vessels by control over their growth, development and remodeling. Active reaction of the smooth muscle cells in the wall is determined by the shear stress at the inner surface of the vessel. Mechanical factors are involved in development of different pathologies as fat and calcium deposition in the wall and the plaque formation, wall thickening, age-induces arteriosclerosis, occlusion of the vessel and ischemia of the organ or its separate parts.

When hydrostatic pressure in the vessel becomes lower then the pressure in the surrounding tissue, the lumen area and the flow rate through the tube decrease. Stability of the vessel wall and development of the collapse significantly depend on the mechanical properties and structure of the wall. Fluid-structure interaction in a stenosed artery can generate oscillations of the downstream arterial wall. Sound produced by the oscillations can be used as a diagnostic tool for detecting stenosed parts of the arteries. Although there is an extensive literature on arterial wall mechanics, our understanding is still far from complete.

Stability of different wall modes in fluid motion through a uniform compliant tube has been comprehensively investigated in both theoretical models and experimental studies [1–4]. The results revealed that wall mechanics plays an important role in transition from laminar to turbulent flow. Complex structure of the wall and different mechanical properties of its layers can influence stability of the unstable modes. Wall parameters and viscous stress in a single-layered model were found to stabilize the unstable mode [5]. Coupling of the inner and outer layers of the arterial wall can be considered as a reinforced cylindrical shell that might influence stability of the wall modes in comparison with a uniform single-layered case. In the present paper stability of the laminar flow of the viscous incompressible liquid in the multilayered viscoelastic tube as a realistic model of the blood vessel wall is investigated.

2 Three-layered structure of the wall.

The arterial and venous walls are composed of concentric layers with different thicknesses and mechanical properties. The detailed description of the composite structure of the layers is presented in literature [7–9]. Here we concentrate on the recent data on the elastic properties and relative thicknesses of the layers of the arterial wall in normal and pathological states.

2.1 Intima

The innermost layer is called intima. It consists of a mono-layer of endothelium cells separated by a thin basal membrane from the sub-endothelium layer. Thickness of the intima $h_1 \approx 2 - 3\ \mu m$ [10] and in young healthy subjects the intima contributes negligibly to the mechanical properties of the artery. With age and in pathological states its thickness and stiffness may greatly increase. Initial stage of arteriosclerosis is also connected with thickening and stiffening of the intima. In hypertensive patients wall thickening is an adaptive process, that finally reduces the increased wall tension. The corresponding arteries of hypertensive and normotensive individuals have practically similar internal radii ($R = 2.47 \pm 0.32\ \mu m$ and $R = 2.41 \pm 0.35\ \mu m$ ac-

cordingly), whereas thickness of intima relative to the thickness h_2 of the middle layer (h_1/h_2) and wall-to-lumen ratio (h/R) where $h = h_1 + h_2 + h_3$ are significantly increased in the hypertensive patients in comparison with normotensive ones ($h_1/h_2 = 0.268 \pm 0.032$, $h/R = 0.220 \pm 0.038$ and $h_1/h_2 = 0.236 \pm 0.025$, $h/R = 0.195 \pm 0.028$ accordingly) [11]. For porcine femoral and cutaneous arteries $h_1/h = 0.035, h_1/h_2 = 0.05$ [12].

The endothelial cells are sensitive to shear stress τ_w exerted by the blood flow at the wall. For instance, the cells can align themselves in compliance with the direction of the flow. The sensitivity threshold of the endothelial cells is $\tau_w \approx 0.1\ Pa$. The intima passes mechanical stimuli into the middle layer. The active response of the deendothelized and normal arteries on the flow rate differ both in sign and value. When shear rate at the wall increases due to increasing the blood viscosity from 2.5 to 4.0 $mPa \cdot s$, the Young's modulus of the sheep brachiocephalic artery decreases from $E = 3.11\ MPa$ to $E = 2.09\ MPa$ for the intact artery and increases from $E = 3.16\ MPa$ to $E = 4.1\ MPa$ for the deendothelized artery. Elasticity of the intact artery is defined by the middle layer mainly [13].

2.2 Media

The middle layer makes up the greatest volume of the artery and is responsible for most of its mechanical properties. The media consists of a complex three-dimensional network of elastin and collagen fibers, smooth muscle cells (SMC) and proteoglycans. SMC has a nearly circumferential orientation in most vessels and, when activated, alters circumferential mechanical properties by constricting or dilating. SMC role is very important in maintaining the pressure-flow relation in the vessel by increasing (decreasing) the stress in the wall and decreasing (increasing) the lumen in response to increasing (decreasing) the blood pressure. SMC contraction as a response to decreasing the shear rate at the wall is stimulated by the endothelium cells.

The media is separated into several concentric fiber-reinforced layers by the elastic laminae. The number of laminae as well as the inner radius of the vessel gradually decreases from the aorta toward the periphery arteries. Some arteries exhibit a significant correlation between the thickness of the wall h and the media layer h_2 [13]. For porcine femoral and cutaneous arteries the relative thickness of the media $h_2/h = 0.760$ have been found [12].

2.3 Adventitia

The outermost layer is called adventitia. It consists of thick bundles of collagen fibers, some elastin fibers, fibroblasts, nerves and an intravascular bed (the vasa vasorum). The adventitia influences the mechanical properties mainly by facilitating

tethering to the surrounding tissue and by limiting the lumen increase and damage of the vessel at high internal pressures. Media and adventitia can be considered as fiber-reinforced composites due to the helical structure formed by the collagen microfibrils [9].

Relative thickness of the adventitia depends on the type and position of the blood vessel. In muscular arteries adventitia and media are of the same thickness whereas in elastic arteries and in arterioles it is thin. In cerebral arteries adventitia is practically absent. For coronary artery with wall thickness $h = 1 \pm 0.2\ mm$ the total thickness of intima and media is $h_1 + h_2 = 0.34 \pm 0.1\ mm$ and of adventitia is $h_3 = 0.54 \pm 0.2\ mm$ [14]. For porcine arteries $h_3/h = 0.205$ [12].

3 Mechanical properties and material parameters of the layers

Experiments with arteries and arterial segments revealed that the vessel wall exhibits creep, stress relaxation, hysteresis of the stress-strain relationship that characterize its viscoelastic properties which are quite insensitive to the rate of the imposed strain. Vessel walls exhibit nonlinear stress-strain dependence, with higher extensibility in the low stretch range and progressively decreasing extensibility with increasing stretch. Mechanical properties of passive vessels are defined by parallel arrangement of elastin and collagen fibers with linear elasticity and circular arrangement of SMC in the media. Due to the SMC the wall behaves differently in the passive and activated states.

The wall material can be treated as compressible when studying fluid motion within the porous wall, but is considered as incompressible when studying macroscopic characteristics on a large time-scale when fluid exchanges between the blood and the wall can be neglected [15–17]. The wall has different mechanical properties in axial and radial directions and can be modeled as anisotropic material [17]. Due to geometry of the vessel it can be modeled as cylindrically orthotropic thick-walled three-layered tube made of nonlinear viscoelastic material.

The Young's modulus E_j and shear modulus G_j of separate layers and entire wall E, G have been obtained for different types of arteries with different radiuses that makes difficult the comparative study of the material parameters. The shear modulus of the wall does not satisfy the relation between the Young's modulus and Poisson's ratio ν of the classical elasticity theory $G = E/(2(1+\nu))$ [18], so the wall material is not isotropic and its properties in radial and circumferential directions differs from its properties in longitudinal direction.

Normally vessels are stretched and fastened to the outer tissues that increases

their stiffness. Shear modulus of the rat thoracic aorta under physiological pressures significantly depends on the longitudinal extension λ_z and circumferential stress $\sigma_{\theta\theta}$. For the rat aorta $G = 183 \pm 25$ kPa at physiological conditions ($P = 16$ kPa, $\lambda_z = 1.3$) [18]. For the porcine left and right coronary arteries $G = 210 \pm 46.5$ and $G = 231 \pm 55.1$ kPa, respectively at physiological conditions ($P = 13.3$ kPa, $\lambda_z = 1.4$). Experimental study of both rat aorta and porcine coronary artery revealed that shear modulus does not depend on the shear strain or stress and linearly depends on the circumferential and longitudinal stresses and in a nonlinear way on the corresponding strains [18–19]. Linear regression coefficients of the relationship $G = \alpha + \beta\sigma_{\theta\theta}$ have been calculated for $\lambda_z = 1.2 \div 1.4$ [18]. The incremental Young's modulus for human ascending aorta is 33-360 kPa [20]. In bovine and rabbit aorta the tangential Young's modulus is approximately 20 times greater than the radial modulus. [16].

The relationship between Kirchhoff stress and Green's strain is approximately linear within the physiological range for canine pulmonary arteries [21] up to the axial and circumferential elongations $\lambda_z = 1.5 - 1.6$ and $\lambda_\theta = 1.7 - 1.8$ that includes the physiological region which does not exceed $\lambda_z \approx 1.2$ due to the longitudinal tethering of the vessels [22]. The stress-strain curves can be considered as linear when the pressure in the vessel is less than 60 mmHg and as nonlinear with strain-dependent elasticity modulus for the greater pressures [16]. In spite the tethering the length of the common carotid artery varies during the cardiac cycle and its movement is inversely correlated with pulse pressure [23].

Within the framework of the anisotropic single-phase model of the longitudinally non-stretched wall the Young's modulus and Poisson's ratio in the plane of isotropy (E_1, ν_1) and in the perpendicular direction (E_2, ν_2) are $E_1 = 460\ kPa$, $E_2 = 20\ kPa$, $\nu_1 = 0.3$, $\nu_2 \in [0; 0.05]$. Within the physiological pressure range when the wall volume remains constant, $\nu_2 = 0.038$ [16,25].

As the intima is a very thin layer, the inner layer as a composition of the intima and media is often investigated in experiments and compared to the outer layer or adventitia. In superficial arteries transcutaneous ultrasonography gives the values of total arterial wall and media thickness that correspond to histological data [12]. The method is less accurate for estimation the thickness of both the adventitia and intima layers so reliable determination of thicknesses of the layers are available by histological examination.

The inner and outer layers of the artery work at different mechanical conditions. When the internal and external pressures and longitudinal stress are zero then the inner layer is under compression and the outer layer is in tension, and the value of compressive stress is greater than the tensile stress [26]. The pressure-diameter relationships are different for normal vessel segment and for the same segment after being turned inside out because of different initial strain distributions in the wall

[27].

The Young's modulus of the adventitia is lower then that of the media. For the porcine thoracic aorta the Young's modulus $E_{i,o}$ of the inner and outer layers accordingly are $E_i = 16.054 - 55.474\ kPa$, $E_o = 2.91 - 6.65\ kPa$ with $E_i/E_o = 5.53 - 16.33$ [28]. The Young's modulus of the intima-media and the adventitia layers of the pig thoracic aorta are $E = 43.2 \pm 15.8\ kPa$, $E = 4.7 \pm 1.72\ kPa$ in a linear range of the stress-strain curve including both the zero-stress state and the no-load state.

The experimental results confirm the important role of mechanical properties and geometry of the layers in the function, growth, stability and development of pathology of the blood vessels. Basing on the presented data stability of the blood flow in the vessel is considered in the next sections as a 3D flow of the viscous liquid in the three-layered tube. In this study material of the tube is treated as viscoelastic anisotropic. Active stress in the middle layer, initial stretching of the vessel and residual stress in the wall [29] are not taken into consideration though they play a significant role in the wall dynamics as it was shown in this section. Including the active response and the pre-stretching of the vessels will be the subject of the future investigations on the topic.

4 Governing equations

The flow in the blood vessels of alive bodies are approximated in this paper by a flow in a long viscoelastic multilayerd non-isotropic thick-walled tube with the inner radius R, thickness h and length L ($R/L << 1$) as it is sketched in figure 1. The continuity and Navier-Stokes equations governing the fluid motion are :

$$\nabla \cdot \vec{v}^* = 0 \tag{1}$$

$$\frac{\partial \vec{v}^*}{\partial t} + \vec{v}^* \cdot \nabla \vec{v}^* = -\frac{1}{\rho_f} \nabla p^* + \frac{1}{\rho_f} \nabla \cdot \hat{\sigma}^* \tag{2}$$

where $\vec{v}^*$ is the fluid velocity, ρ_f is the fluid mass density, p^* is the hydrostatic pressure and $\hat{\sigma}^*$ is the viscous stress tensor in the fluid. When wall material is considered as incompressible then the mass conservation and momentum equations can be written as :

$$\nabla \cdot \vec{u}^{*j} = 0 \tag{3}$$

$$\rho_w^j \frac{\partial^2 \vec{u}^{*j}}{\partial t^2} = -\nabla p^{*j} + \nabla \cdot \hat{\sigma}^{*\mathbf{j}} \tag{4}$$

where $\vec{u}^{*j}$, p^{*j}, ρ_w^{*j}, $\hat{\sigma}^{*\mathbf{j}}$ are the displacement, pressure, mass density and the stress tensor for the j-th layer of the wall, $j = 1, 2, 3$. The boundary conditions include

the continuity conditions for the fluid velocity and displacement of the inner layer and normal and shear stresses at the inner wall; the continuity conditions at the interfaces of the layers; the no displacement conditions at the tethered outer surface of the vessel respectively :

$$r^* = R: \quad \vec{v}^* = \frac{\partial \vec{u}^{*1}}{\partial t}, \quad \hat{\sigma}^{*\mathbf{1}}_{\mathbf{n}} = \hat{\sigma}^*_{\mathbf{n}} \tag{5}$$

$$r^* = R + h_1: \quad \vec{u}^{*1} = \vec{u}^{*2}, \quad \hat{\sigma}^{*\mathbf{1}}_{\mathbf{n}} = \hat{\sigma}^{*\mathbf{2}}_{\mathbf{n}} \tag{6}$$

$$r^* = R + h_1 + h_2: \quad \vec{u}^{*2} = \vec{u}^{*3}, \quad \hat{\sigma}^{*\mathbf{2}}_{\mathbf{n}} = \hat{\sigma}^{*\mathbf{3}}_{\mathbf{n}} \tag{7}$$

$$r^* = R + h: \quad \vec{u}^{*3} = 0 \tag{8}$$

where n denotes the component of the stress tensor which is orthogonal to the corresponding interface.

For the viscoelastic layers with parallel connection of the elastic and viscous elements [30] the constitutive equations are

$$\vec{\sigma}^j_i = A^j_{ik}\varepsilon^j_k + \mu^j_w \frac{\partial}{\partial t}\vec{\varepsilon}^j_i \tag{9}$$

where

$$\vec{\sigma}^{*jT} = (\sigma^*_{r^*r^*}, \sigma^*_{\theta\theta}, \sigma^*_{z^*z^*}, \sigma^*_{\theta z^*}, \sigma^*_{r^*z^*}, \sigma^*_{r^*\theta})$$

$$\vec{\varepsilon}^{*jT} = (\varepsilon^*_{r^*r^*}, \varepsilon^*_{\theta\theta}, \varepsilon^*_{z^*z^*}, \varepsilon^*_{\theta z^*}, \varepsilon^*_{r^*z^*}, \varepsilon^*_{r^*\theta})$$

and the quantities $(\varepsilon^*_{r^*r^*}, \varepsilon^*_{\theta\theta}, \varepsilon^*_{z^*z^*}, \varepsilon^*_{\theta z^*}, \varepsilon^*_{r^*z^*}, \varepsilon^*_{r^*\theta})$ are the components of the strain tensor

$$\hat{\varepsilon}^{*j} = \frac{1}{2}(\nabla \vec{u}^{*j} + \nabla \vec{u}^{*jT}) \tag{10}$$

and $(\sigma^*_{r^*r^*}, \sigma^*_{\theta\theta}, \sigma^*_{z^*z^*}, \sigma^*_{\theta z^*}, \sigma^*_{r^*z^*}, \sigma^*_{r^*\theta})$ are the components of the stress tensor $\hat{\sigma}^{*\mathbf{j}}$ in cylindrical co-ordinates (r^*, θ, z^*), A^j_{ik} is the matrix of elasticity coefficients, μ^j_w are the viscosities of the layers.

When the material is considered as transversely isotropic and the plane of isotropy is perpendicular to the r-axis [16] then

$$(A^j_{ik})^{-1} = \begin{pmatrix} \frac{1}{E^j_2} & \frac{-\nu^j_2}{E^j_2} & \frac{-\nu^j_2}{E^j_2} & 0 & 0 & 0 \\ \frac{-\nu^j_2}{E^j_2} & \frac{1}{E^j_1} & \frac{-\nu^j_1}{E^j_1} & 0 & 0 & 0 \\ \frac{-\nu^j_2}{E^j_2} & \frac{-\nu^j_1}{E^j_1} & \frac{1}{E^j_1} & 0 & 0 & 0 \\ 0 & 0 & 0 & \frac{1}{2G^j} & 0 & 0 \\ 0 & 0 & 0 & 0 & \frac{1}{2G^j} & 0 \\ 0 & 0 & 0 & 0 & 0 & \frac{1}{2G^j} \end{pmatrix}$$

For an isotropic material when $E_1^j = E_2^j = E^j$, $\nu_1^j = \nu_2^j = \nu^j$, the problem (1)–(8) can be considered for a two-layered tube (the inner and outer layers) taking into considerations the data for E_i and E_o [28]. For an isotropic viscoelastic material stability of the system has been investigated for axisymmetric [3] and non-axisymmetric [4–5] small perturbations. To present day possible investigation of the three-layered anisotropic blood vessels has been restricted by absence of the precise data on viscous and elastic parameters of the layers.

5 First order system of differential equations controlling a normal mode

>From now and in what follows we shall use a dimensionless variables where the distance will be scaled by the tube radius R, the velocity by $V_{ref} = (G_{ref}/\rho_f)^{1/2}$ where G_{ref} is a reference shear modulus which will be chosen to be of the same order of magnitude of the shear modulus of one viscoelastic layer forming the tube. The shear modulus of all the layers will be scaled by G_{ref}. The solid mass density will be scaled by the fluid mass density ρ_f and $\rho_r^i = \rho_w^i/\rho_f$ are the solid/fluid density ratios. The time scale is $(\rho_f R^2/G_{ref})^{1/2}$. The Young's modulus will be scaled by G_{ref}, to say, ${\Xi_1}^j = E_1^j/G_{ref}$, ${\Xi_2}^j = E_2^j/G_{ref}$, the pressure will be scaled by G_{ref}. The solid viscosity, μ_w, well be scaled by the fluid viscosity μ_f and $\mu_r^j = \mu_w^j/\mu_f$ stands for the relative solid/fluid viscosity. Let V_r be the maximum value of the velocity of the basic steady flow. We introduce $\Gamma = (\rho_f V_r^2/G_{ref})^{1/2} = V_r/V_{ref}$ which is the ratio of the inertial fluid forces to the elastic solid forces or the ratio of the basic flow speed to the characteristic solid wave speed. The wall of the tube consisted of three layers with dimensionless thicknesses $H_j = h_j/R, j = 1-3$ with different mechanical properties, see figure 1. The relative thickness of the wall is $H = h/R$.

We suppose that before the system is being disturbed, the three-layered viscoelastic tube is in a dynamic equilibrium with the conveyed steady flow. The steady velocity field in the fluid has a unique component parallel to the axis of the tube, namely :

$$\vec{v_b} = V_f^* \vec{e}_z = V_r V_f \vec{e}_z = V_{ref} \Gamma V_f \vec{e}_z \tag{11}$$

Furthermore, we suppose that the steady axial velocity component $V_f = V_f(r)$ depends only on the radial distance. Let $\vec{v}$, p be a dimensionless velocity and pressure disturbances which we add to the basic velocity and pressure fields $\vec{v_b}$, p_b in such a way, the instantaneous fields are $\vec{v^*} = \vec{v_b} + V_{ref}\vec{v}$ and $p^* = p_b + p\ G_{ref}$. Then, neglecting the nonlinear terms in (1)-(2) leads to the following system of partial differential linear equations controlling the evolution of any infinitesimal disturbance which read

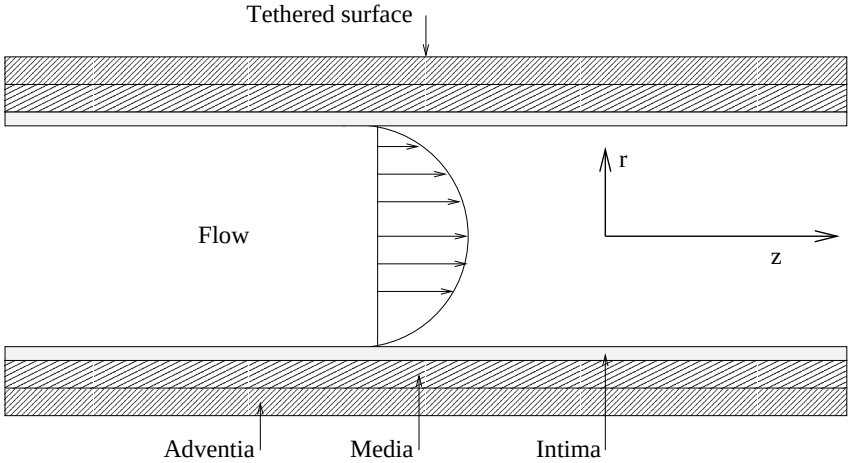

FIG. 1 – Coordinate system and tube in non-disturbed state

$$\nabla \cdot \vec{v} = 0 \tag{12}$$

$$\frac{\partial \vec{v}}{\partial t} + V_f \frac{\partial \vec{v}}{\partial z} + v_r \frac{dV_f}{dr}\vec{e}_z = -\nabla p + \frac{\Gamma}{Re}\nabla \cdot \hat{\sigma} \tag{13}$$

where $Re = \rho_f V_r R/\mu_f$ is the Reynolds number, $\hat{\sigma}$ is dimensionless viscous stress tensor in the fluid. The dynamic equations in the solid (4) are not modified as far as we consider the small disturbances. However, the boundary conditions (5) at the fluid/solid interface have to be reconsidered, indeed, the continuity of the velocity field at the interface can be written in the form :

$$r = 1 + u_r^1 : \quad V_f(r)\vec{e}_z + \vec{v} = \frac{\partial \vec{u}^1}{\partial t} \tag{14}$$

where $u_r = u_r^*/R$ is the radial dimensionless displacement of the material point located at the interface. A Taylor expansion of $V_f(1 + u_r)$ in the vicinity of the dynamic equilibrium position located at $r = 1$ and the fact that $V_f(1) = 0$ allows the boundary condition (14) to be considered in the form

$$r = 1 : \quad u_r^1 \frac{dV_f(r)}{dr}\vec{e}_z + \vec{v} = \frac{\partial \vec{u}^1}{\partial t} \tag{15}$$

Since the coefficients of the partial differential equations are independent of the azimuthal and axial coordinates the solution of the problem (1)-(9) in the non-dimensionalized form can be sought in the form of a normal mode :

$$(v_j, p_f) = (\tilde{v}_j, \tilde{p}_f)e^{st+ikz+in\theta} + cc \tag{16}$$

$$(u_j, p_s) = (\tilde{u}_j, \tilde{p}_s)e^{st+ikz+in\theta} + cc \tag{17}$$

where v_j, u_j, p_f, p_s are the velocity, displacement and pressure disturbances, cc denote complex conjugate. By substituting (16)-(17) into (4), (12) and (13) one can obtain a system of differential equations for the disturbances in the fluid :

$$\frac{d\tilde{v}_r}{dr} = \Lambda \quad ; \quad \frac{d\tilde{v}_\theta}{dr} = \tilde{\xi}_\theta \quad ; \quad \frac{d\tilde{v}_z}{dr} = \tilde{\xi}_z \tag{18}$$

$$\Lambda = -\frac{\tilde{v}_r}{r} - in\frac{\tilde{v}_\theta}{r} - ik\tilde{v}_z \tag{19}$$

$$\frac{d\tilde{p}_f}{dr} = -ik\tilde{V}_f\tilde{v}_r - s\tilde{v}_r + \frac{d\tilde{\sigma}_{rr}}{dr} + \frac{\tilde{\sigma}_{rr}}{r} + \frac{in}{r}\tilde{\sigma}_{r\theta} + ik\tilde{\sigma}_{rz} - \frac{\tilde{\sigma}_{\theta\theta}}{r} \tag{20}$$

$$\frac{d\tilde{\xi}_\theta}{dr} = -\frac{in}{r}\Lambda + \frac{in\tilde{v}_r}{r^2} - \frac{\tilde{v}_\theta}{r^2} + \frac{1}{r}\tilde{\xi}_\theta + Re\Gamma^{-1}[+ik\tilde{V}_f\tilde{v}_\theta + s\tilde{u}_\theta + \frac{in}{r}\tilde{p}_f$$

$$-\frac{in}{r}\tilde{\sigma}_{\theta\theta} - ik\tilde{\sigma}_{\theta z} - \frac{\tilde{\sigma}_{r\theta}+\tilde{\sigma}_{\theta r}}{r}]$$

$$\frac{d\tilde{\xi}_z}{dr} = -ik\Lambda + Re\Gamma^{-1}[+ik\tilde{V}_f\tilde{v}_z + \tilde{v}_r\frac{d\tilde{V}_f}{dr} + s\tilde{v}_z + ik\tilde{p}_f - \frac{\tilde{\sigma}_{zr}}{r} - \frac{in}{r}\tilde{\sigma}_{z\theta} - ik\tilde{\sigma}_{zz}]$$

$$\begin{pmatrix} \tilde{\sigma}_{rr} & \tilde{\sigma}_{r\theta} & \tilde{\sigma}_{rz} \\ \tilde{\sigma}_{\theta r} & \tilde{\sigma}_{\theta\theta} & \tilde{\sigma}_{\theta z} \\ \tilde{\sigma}_{zr} & \tilde{\sigma}_{z\theta} & \tilde{\sigma}_{z\theta} \end{pmatrix} = \frac{\Gamma}{Re}\begin{pmatrix} 2\Lambda & \tilde{\xi}_\theta + \frac{in\tilde{v}_r}{r} - \frac{\tilde{v}_\theta}{r} & \tilde{\xi}_z + ik\tilde{v}_r \\ \tilde{\xi}_\theta + \frac{in\tilde{v}_r}{r} - \frac{\tilde{v}_\theta}{r} & 2(\frac{in\tilde{v}_\theta}{r} + \frac{\tilde{v}_r}{r}) & \frac{in\tilde{v}_z}{r} + ik\tilde{v}_\theta \\ \tilde{\xi}_z + ik\tilde{v}_r & \frac{in\tilde{v}_z}{r} + ik\tilde{v}_\theta & 2ik\tilde{v}_z \end{pmatrix}$$

and in the solid media :

$$\frac{d\tilde{u}_r}{dr} = \Upsilon_1 \quad ; \quad \frac{d\tilde{u}_\theta}{dr} = \tilde{\zeta}_\theta \quad ; \quad \frac{d\tilde{u}_z}{dr} = \tilde{\zeta}_z \tag{21}$$

$$\begin{aligned}\frac{d\tilde{p}_s}{dr} = -\rho_r s^2\tilde{u}_r + \frac{d\tilde{T}_{rr}}{dr} + \frac{\tilde{T}_{rr}}{r} + \frac{in}{r}\tilde{T}_{r\theta} + ik\tilde{T}_{rz} - \frac{\tilde{T}_{\theta\theta}}{r} \\ + \frac{d\tilde{D}_{rr}}{dr} + \frac{\tilde{D}_{rr}}{r} + \frac{in}{r}\tilde{D}_{r\theta} + ik\tilde{D}_{rz} - \frac{\tilde{D}_{\theta\theta}}{r}\end{aligned} \tag{22}$$

$$\frac{d\tilde{\zeta}_\theta}{dr} = -\frac{in}{r}\Upsilon_1 + \frac{in\tilde{u}_r}{r^2} - \frac{\tilde{u}_\theta}{r^2} + \frac{1}{r}\tilde{\zeta}_\theta + (\Theta + Re^{-1}\Gamma s\mu_r)^{-1}[\rho_r s^2\tilde{u}_\theta + \frac{in}{r}\tilde{p}_s$$

$$-\frac{in}{r}\tilde{T}_{\theta\theta} - ik\tilde{T}_{\theta z} - \frac{\tilde{T}_{r\theta}+\tilde{T}_{\theta r}}{r} - \frac{in}{r}\tilde{D}_{\theta\theta} - ik\tilde{D}_{\theta z} - \frac{\tilde{D}_{r\theta}+\tilde{D}_{\theta r}}{r}]$$

$$\frac{d\tilde{\zeta}_z}{dr} = -ik\Upsilon_1 + (\Theta + Re^{-1}\Gamma s\mu_r)^{-1}[\rho_r s^2\tilde{u}_z + ik\tilde{p}_s - \frac{\tilde{T}_{zr}}{r} - \frac{in}{r}\tilde{T}_{z\theta} - ik\tilde{T}_{zz}$$

$$-\frac{\tilde{D}_{zr}}{r} - \frac{in}{r}\tilde{D}_{z\theta} - ik\tilde{D}_{zz}]$$

$$\begin{pmatrix} \tilde{D}_{rr} & \tilde{D}_{r\theta} & \tilde{D}_{rz} \\ \tilde{D}_{\theta r} & \tilde{D}_{\theta\theta} & \tilde{D}_{\theta z} \\ \tilde{D}_{zr} & \tilde{D}_{z\theta} & \tilde{D}_{z\theta} \end{pmatrix} = \kappa\begin{pmatrix} 2\Upsilon_1 & \tilde{\zeta}_\theta + r^{-1}(in\tilde{u}_r - \tilde{u}_\theta) & \tilde{\zeta}_z + ik\tilde{u}_r \\ \tilde{\zeta}_\theta + \frac{in\tilde{u}_r - \tilde{u}_\theta}{r} & \frac{in\tilde{u}_\theta + \tilde{u}_r}{2r} & in\frac{\tilde{u}_z}{r} + ik\tilde{u}_\theta \\ \tilde{\zeta}_z + ik\tilde{u}_r & inr^{-1}\tilde{u}_z + ik\tilde{u}_\theta & 2ik\tilde{u}_z \end{pmatrix}$$

$$\kappa = Re^{-1}\Gamma s\mu_r$$

$$\begin{pmatrix} \Upsilon_1 \\ r^{-1}(in\tilde{u}_\theta + \tilde{u}_r) \\ ik\tilde{u}_z \\ \tilde{\zeta}_\theta + r^{-1}(in\tilde{u}_r - \tilde{u}_\theta) \\ inr^{-1}\tilde{u}_z + ik\tilde{u}_\theta \\ \tilde{\zeta}_z + ik\tilde{u}_r \end{pmatrix} = \begin{pmatrix} \frac{1}{\Xi_2} & \frac{-\nu_2}{\Xi_2} & \frac{-\nu_2}{\Xi_2} & 0 & 0 & 0 \\ \frac{-\nu_2}{\Xi_2} & \frac{1}{\Xi_1} & \frac{-\nu_1}{\Xi_1} & 0 & 0 & 0 \\ \frac{-\nu_2}{\Xi_2} & \frac{-\nu_1}{\Xi_1} & \frac{1}{\Xi_1} & 0 & 0 & 0 \\ 0 & 0 & 0 & \Theta & 0 & 0 \\ 0 & 0 & 0 & 0 & \Theta & 0 \\ 0 & 0 & 0 & 0 & 0 & \Theta \end{pmatrix} \begin{pmatrix} \tilde{T}_{rr} \\ \tilde{T}_{\theta\theta} \\ \tilde{T}_{zz} \\ \tilde{T}_{r\theta} \\ \tilde{T}_{\theta z} \\ \tilde{T}_{rz} \end{pmatrix}$$

The relation between the derivatives of the diagonal stress tensor components and the components of the displacement vector and their first order derivatives d/dr are

$$\Upsilon_1 = -\frac{\tilde{u}_r}{r} - in\frac{\tilde{u}_\theta}{r} - ik\tilde{u}_z$$

$$\begin{pmatrix} \Upsilon_2 \\ r^{-2}(-in\tilde{u}_\theta - \tilde{u}_r) + r^{-1}(in\tilde{\zeta}_\theta + \Upsilon_1) \\ ik\tilde{\zeta}_z \end{pmatrix} = \begin{pmatrix} \frac{1}{\Xi_2} & \frac{-\nu_2}{\Xi_2} & \frac{-\nu_2}{\Xi_2} \\ \frac{-\nu_2}{\Xi_2} & \frac{1}{\Xi_1} & \frac{-\nu_1}{\Xi_1} \\ \frac{-\nu_2}{\Xi_2} & \frac{-\nu_1}{\Xi_1} & \frac{1}{\Xi_1} \end{pmatrix} \begin{pmatrix} \frac{d\tilde{T}_{rr}}{dr} \\ \frac{d\tilde{T}_{\theta\theta}}{dr} \\ \frac{d\tilde{T}_{zz}}{dr} \end{pmatrix}$$

where

$$\Upsilon_2 = +\frac{\tilde{u}_r}{r^2} - \frac{1}{r}\Upsilon_1 - \frac{in}{r}\tilde{\zeta}_\theta + in\frac{\tilde{u}_\theta}{r^2} - ik\tilde{\zeta}_z \tag{23}$$

The boundary conditions for the disturbances are

$$\text{at} \quad r = 0: \qquad \widetilde{v}_r \ = 0 \quad ; \quad \frac{d\widetilde{v}_x}{dr} = 0 \tag{24}$$

$$\text{at} \quad r = 1: \qquad \tilde{v}_r \ = s\tilde{u}_r^1 \quad ; \quad \tilde{v}_x + \frac{dV_f(r)}{dr}\tilde{u}_r^1 = s\tilde{u}_x^1 \tag{25}$$

$$-\tilde{p}_s^1 + \tilde{T}_{rr}^1 + \tilde{D}_{rr}^1 = -\tilde{p}_f + \tilde{\sigma}_{rr} \tag{26}$$

$$\tilde{T}_{rx}^1 + \tilde{D}_{rx}^1 = \tilde{\sigma}_{rx} \tag{27}$$

at the interfaces between the j-th and j+1-th layers, j=1,2 :

$$\tilde{u}_r^j \ = \tilde{u}_r^{j+1} \quad ; \quad \tilde{u}_x^j = \tilde{u}_x^{j+1} \tag{28}$$

$$-\tilde{p}_s^j + \tilde{T}_{rr}^j + \tilde{D}_{rr}^j = -\tilde{p}_s^{j+1} + \tilde{T}_{rr}^{j+1} + \tilde{D}_{rr}^{j+1} \tag{29}$$

$$\tilde{T}_{rx}^j + \tilde{D}_{rx}^j = \tilde{T}_{rx}^{j+1} + \tilde{D}_{rx}^{j+1} \tag{30}$$

$$\text{at} \quad r = 1 + H: \qquad \tilde{u}_r^3 \ = 0 \quad ; \quad \tilde{u}_x^3 = 0 \tag{31}$$

The first-order differential equations for axisymmetric disturbances can easily be obtained by substituting $n = 0$ into (18)–(31).

6 Numerical method

By substituting $n = 0$, $\tilde{v}_\theta = 0$, $\tilde{u}_\theta = 0$ into (18)–(31) we obtain the system of first-order differential equations that can be solved using a fourth-order Runge–Kutta method. Therefore two independent solutions ($\mathbf{X}_1$,$\mathbf{X}_2$) where each one satisfies the boundary conditions at $r = 0$ have been obtained in the fluid medium. The components of the vectors $\mathbf{X}_i$, $i = 1, 2$ are the velocity components and their first order derivatives d/dr and the pressure in the fluid. The independence of the two solutions, $\mathbf{X}_i$, is ensured by starting the computation with one of the two independent vectors formed by several values of the vector $(\tilde{v}_x, \tilde{p}_f)$ at $r = 0$. For instance $\mathbf{X}_1$ can be obtained by starting the computation with the boundary condition

$$\mathbf{X}_1 = (\tilde{v}_x, \tilde{v}_r, \tilde{p}_f, \tilde{\xi}_r, \tilde{\xi}_x)^T = (1, 0, 0, 0, 0)^T \qquad ; \qquad \text{at } r = 0$$

and $\mathbf{X}_2$ can be obtained by starting the computation with the boundary condition

$$\mathbf{X}_2 = (\tilde{v}_x, \tilde{v}_r, \tilde{p}_f, \tilde{\xi}_r, \tilde{\xi}_x)^T = (0, 0, 1, 0, 0)^T \qquad ; \qquad \text{at } r = 0$$

by this choice the boundary conditions at $r = 0$ are taken into consideration by both solution, namely $\mathbf{X}_1$ and $\mathbf{X}_2$. Note that the chosen values at $r = 0$ must form a set of independent vectors which is sufficient for $\mathbf{X}_1$ and $\mathbf{X}_2$ to be independent vectors. Then the general solution in the fluid medium is a linear combination of the two independent solutions $\mathbf{X}_1$ and $\mathbf{X}_2$, such that

$$\mathbf{Z}_1 = A_1\mathbf{X}_1 + A_2\mathbf{X}_2 \tag{32}$$

where (A_1,A_2) are arbitrary constants.

Similarly, for the displacement field in the solid, we solve the system for two independent solutions ($\mathbf{Y}_1$,$\mathbf{Y}_2$) where each one satisfies the boundary conditions at $r = H$. The components of the vectors $\mathbf{Y}_1, \mathbf{Y}_2$ are the components of the displacement vector and their first order derivatives d/dr and the pressure in the solid medium. The independence of the solutions is ensured by starting the computation with one of the two independent values of the vector $(\tilde{\zeta}_x, \tilde{p}_s)$ at $r = 1 + H$. For instance $\mathbf{Y}_1$ can be obtained by starting the computation with the boundary condition

$$\mathbf{Y}_1 = (\tilde{u}_x, \tilde{u}_r, \tilde{p}_s, \tilde{\zeta}_r, \tilde{\zeta}_x)^T = (0, 0, 0, 0, 1)^T \qquad ; \qquad r = 1 + H$$

and $\mathbf{Y}_2$ can be obtained by starting the computation with the boundary condition

$$\mathbf{Y}_2 = (\tilde{u}_x, \tilde{u}_r, \tilde{p}_s, \tilde{\zeta}_r, \tilde{\zeta}_x)^T = (0, 0, 1, 0, 0)^T \qquad ; \qquad r = 1 + H$$

by this choice the boundary conditions at $r = 1+H$ are considered by both solutions. The chosen values form a set of inependent vectors which ensures the independence

of $\mathbf{Y}_1$ and $\mathbf{Y}_2$. At the interface solid/solid, the boundary conditions are enforced numerically. The general solution in the solid medium is a linear combination of $\mathbf{Y}_1$ and $\mathbf{Y}_2$, such that

$$\mathbf{Z}_2 = B_1\mathbf{Y}_1 + B_2\mathbf{Y}_2 \tag{33}$$

where (B_1,B_2) are arbitrary constants. The boundary conditions at $r = 1$ leads to the eigenvalue problem

$$\mathbf{M}\,\mathbf{C} = 0 \tag{34}$$

where $\mathbf{C}^T = (A_1, A_2, B_1, B_2)$ and the elements of the 4×4 matrix $\mathbf{M}$ are the linear combinations of the particular solutions ($\mathbf{X}_1$,$\mathbf{X}_2$), ($\mathbf{Y}_1$,$\mathbf{Y}_2$) and their derivatives d/dr at $r = 1$. The components of the matrix $\mathbf{M}$ include all the parameters of the system directly or via the solutions ($\mathbf{X}_1$,$\mathbf{X}_2$), ($\mathbf{Y}_1$,$\mathbf{Y}_2$). The characteristic equation is obtained by setting $det(\mathbf{M}) = 0$.

7 Eigenvalue Search Technique

In order to solve the equation $det(\mathbf{M}) = 0$ we sweep the complex (s_i, s_r)-plane when the temporal eigenvalues are being sought and accordingly the complex (k_i, k_r)-plane when the spatial eigenvalues are being sought. Here s_r is the amplification rate, s_i is the frequency, k_i is the spatial amplification rate, k_r is the wave number. For this task the complex plane has been divided into a set of large number of small cells. The edges of the cells are used as initial conditions for the best-decent method to converge toward the eigenvalues. The method leads to a large number of repeated modes because the code may converge toward the same eigenvalue for several initial conditions. Thus during the numerical procedure one has to ignore the repeated eigenvalues.

8 Results and discussions

Since the stability of the flow in non-isotropic viscoelastic multi-layered tube as a model of the blood flow in the vessels is considered, the independent material parameters in (18)–(31) have been chosen within the physiological range that is discussed in the sections 2-3. Thus, the temporal and spatial eigenvalues of the system depend on 24 dimensionless geometrical and material parameters namely H_j, ρ_r^j, μ_r^j, $\Xi_{1,2}^j$, G^j, $\nu_{1,2}^j$, $j = 1, 2, 3$. Two dimensionless dynamical parameters Re and Γ represent the ratio of the inertia fluid forces to the fluid viscous forces and to the solid elastic forces accordingly.

An extensive and primitive examination of all possible combinations of these parameters in the model leads to a too large number of figures to be included in

one paper. Therefore, we will focus our attention on the most important of them in order to see the effect of the non-isotropic part of the constitutive equations. First of all we examine the effect of exchanging Young's modulus Ξ_1^j and Ξ_2^j. In figure 2a the temporal eigenvalues in the complex (s_r, s_i)-plane for two values of dimensionless Young's modulus $\Xi_1^j = 2G$, $\Xi_2^j = 20G$ and $\Xi_1^j = 20G$, $\Xi_2^j = 2G$ are presented. The other parameters are kept constant. Surprisingly the difference between these two results is negligibly small indicating that the constitutive equation is quasi symmetric with respect to Ξ_1^j and Ξ_2^j at least for the case which has been considered here. Note that in this case there are two unstable modes at low frequencies as it has been shown in figure 2.

In figure 2b the amplification rate of the most unstable mode versus the Poisson coefficients ν_2^i and ν_1^i is plotted. We can conclude that the amplification rate changes slightly when the Poisson coefficients ν_2^j and ν_1^j vary, indicating that the extra diagonal components in the linear elasticity matrix are not very important in the generation of axisymmetric instabilities. Note that in figure 2b the variation of the coefficients ν_2^j or ν_1^j has been undertaken simultaneously and kept the same in each layer. The effect of the variation of the Poisson coefficient only in one layer has been also examined. The result indicates that alternation of the amplification rate due to the variation of the Poisson coefficients may be ignored. In all the numerical experiments which have been performed here, it has been found that the variation of one of the parameters (ν_2^j, ν_1^j) or ν_2^j and ν_1^j together in any layer has a little effect onto the amplification rate provided that

$$\nu_2^i \neq \pm\sqrt{\frac{\Xi_2^i}{2\Xi_1^i}(1-\nu_1^i)}$$

otherwise the determinant of the linear elasticity matrix is zero and the matrix becomes singular.

The comparative results on the amplification rate of the most unstable mode of isotropic viscoelastic tube and non-isotropic one are presented in figure 3 . The temporal eigenvalues of the isotropic tube form five branches in the (s_i, s_r)-plane. Two branches are localized near the positive imaginary axis (s_i-axis), two others are localized near the negative imaginary axis (s_i-axis) and one branch is localized near the real axis (s_r-axis). The topology of the spectra can easily be understood if one consider the limit case. In fact, if the interface surface between the fluid and the solid is maintained at rest in such a way that there is no interaction between the fluid and the solid. In this virtual state the no-displacement condition for the solid and the no-slip condition for the fluid can be hold at the interface. Furthermore, if we suppose that $Re << 1$, one can replace the Navier-Stokes equations by the Stokes equations. Therefore, in this virtual state one can easily show that the temporal eigenvalues

of the solid layers alone are pure positive or negative imaginary numbers (with zero amplification rate and large frequency range) and the fluid temporal eigenvalues are pure negative real numbers (with zero-frequency and high dampening rate).

When the interaction between the solid and the fluid is allowed, then the solid (fluid) eigenvalues are removed slightly from the imaginary (real) axis. The displacement of the eigenvalues in the (s_i, s_r)-plane, which is a consequence of the fluid-structure interaction, is more effective in the region of the (s_i, s_r)-plane where the frequency and the amplification rate of the solid based modes match the frequency and the amplification rate of the fluid based modes. In fact the interaction is more effective near the origin of the plane (s_i, s_r)-plane which corresponds to the modes of low frequency and low amplification rate.

When the Young's modulus in the radial direction decreases, the amplification rate and dampening rate of the eigenvalues reduce, figure 3 . Furthermore there is another unstable mode with a very small amplification rate. This mode has not been observed in the isotropic case with the same parameters. Note that, as it is shown in figure 2 , diminishing the radial Young's modulus or axial Young's modulus produces approximately the same effect.

The spatial eigenvalues for the isotropic tube and the non-isotropic one are plotted in figure 3b . It is found that the spatial eigenvalues of isotropic tube, indicated by sign + in the figure, form four branches in (k_r, k_i)-plane. The modes with positive (negative) values k_i represent a disturbance localized downstream (upstream) of the source of the disturbance. The spatial eigenvalues for the considered frequency $s_i = 2$ are divided into two groups with low and high wave numbers (relatively long and short waves accordingly). The most striking result for the non-isotropic stress-strain relationship is presented in figure 3b by the shift of the modes toward the long-wave region in (k_r, k_i)-plane (low wave number). Of course, in practical circumstance, the tube is of finite length and tethered at its farthest sections that prohibits the existence of all the waves which length is bigger than the length of the tube. In that way all the modes with $k_r \approx 0$ can not exist in the blood vessels. Note that the fact that k_i is negative or positive does not indicate stability or instability of the system. In fact, the sign of k_i is relevant in the stability of the system only if k cross the real axis in (k_r, k_i)-plane when the amplification rate of the most unstable mode tends to zero. In this circumstance, the value of k_i, when for the most unstable mode $s_r \to 0$, corresponds to spatial amplification rate.

The effect of the simultaneous deviations of different material parameters of all the layers from the isotropic state is illustrated by figures 2–3. Here the relations between the parameters of the layers were kept constant. Now we present the results which have been obtained by variation of the parameters of one layer when the parameters of the other layers were kept constant. We will, particularly, focus our

attention on the group velocity in view of the importance of the speed of the wave propagating in the blood vessels.

The amplification rate of the most unstable mode versus the viscosity of each of the layers is plotted in 4a. Here two cases have been considered when $\Xi_2^j = 2G^j$, $\Xi_1^j = 20G^j$ and $\Xi_1^j = 2G^j$, $\Xi_2^j = 20G^j$ accordingly. In each case the viscosity of two layers are kept constant while the viscosity of the remained one varies. The results presented in figure 4 confirm that exchanging Ξ_2^j and Ξ_1^j in the constitutive equation leads approximately to the same results as it was already obtained in the previous case (see figure 2).

Furthermore, increasing the viscosity of the first layer, which is in contact with the fluid, leads to an increase of the amplification rate of the most unstable mode (figure 4a). Thus, increasing the viscosity of the first layer destabilizes the system. The effect can probably be explained by better fluid-solid coupling when the viscosity of the inner layer is high enough. The viscosity of the second layer show a stabilizing effect (figure 4a) whereas the system is quite indifferent to variation of the viscosity of the third layer. There is no clear explanation of the surprising effect concerning the stabilizing effect of viscosity of the middle layer.

Owing to the fact that the viscosities of the first and second layers have an opposed effect one cannot use the classification suggested by Benjamin (1963) [32] in order to classify this mode in one of the class noted **A**, **B** and **C**. In fact, according to Benjamin's classification, if one considers the total disturbance energy of the coupled fluid–solid system, a decrease in that energy leads to destabilization of the modes of the class **A** and to stabilization of the modes of the class **B** and has no effect on the modes of the class **C**. The effect of the viscosity of the first (second, third) layers suggests that the class **A** (**B**,**C**) is an appropriate one for the corresponding case. Consequently this unstable mode could not belong to any of these classes. Note that the most unstable mode is near the real axis which suggests that the mode is a fluid-based mode and the second unstable mode with small amplification rate is near the imaginary axis which suggests that this is a solid-based mode as it has been shown in [5] using the classification introduced by [33,34].

The group velocity of the most unstable mode versus the viscosity of the layers is presented in figure 4b. Note that when $\mu_r^2 = 0$ the group velocity is negative. Therefore, it is all about an upstream propagated wave. An increase in the viscosity of the first layer, which is in contact with the fluid, leads to an increase in the group velocity. In that way the faster modes have higher viscosities. The variation of the viscosity of the third layer leads to a relatively non-significant alteration in the speed of propagation of the unstable mode. Surprising, any change in the viscosity of the middle layer leads to an inversion of the direction of the propagation of the unstable mode, where the group velocity becomes positive. For some value of μ_r^2 the

group velocity is zero which suggests the existence of absolute instability in the non-isotropic three-layered tube. The existence of such absolute instability in isotropic viscoelastic tubes has been shown in [4].

Influence of the shear modulus and Young's modulus on the most unstable mode is illustrated in figure 5. In each courve the relations $\Xi_2^j = 2G^j$, $\Xi_1^j = 20G^j$ are hold during the computation process. As it is shown in figure 5 the most unstable mode remains unstable for all the considered range of shear modulus. Increasing the shear module of any layer does not stabilize the system. However, the increase in the both shear and Young's modulus has a non-uniform effect on the temporal amplification rate. The variation of the shear modulus of the middle layer G^2 and Young's modulus Ξ_2^2 and Ξ_1^2 when $\Xi_2^2 = 2G^1$, $\Xi_1^2 = 20G^2$ cause an opposite effect in comparison with the variation of the shear modulus of the first layer G^1 subjected to the same conditions. Note that the higher values of the amplification rate have been obtained by the variation of the shear modulus G^2 of the second layer in comparison with the values obtained by variation of the shear modulus G^1 of the first layer (figure 5a). The increase in the shear modulus G^3 of the third layer, subjected to the conditions $\Xi_2^3 = 2G^3$, $\Xi_1^3 = 20G^3$ leads to a relatively small increase in the amplification rate of the most unstable mode

The group velocity of the most unstable mode versus the shear modulus of one layer while the shear modulus of the two other layers are kept constant is plotted in figure 5b. In the same way the Young's modulus is related here to the shear modulus according the conditions $\Xi_2^j = 2G^j$, $\Xi_1^j = 20G^j$, $i = 1, 2, 3$. It was obtained that the group velocity depends in a nonlinear way on the shear modulus. When $G^1 = G^2 = G^3 = 0.1$ the group velocity is negative, so the wave which is formed by the most unstable mode propagates against the flow (the upstream propagated wave). When the shear modulus of the first layer G^1 increases while $G^2 = G^3 = 0.1$, the group velocity of the most unstable mode changes its sign for some values of G^1 and forms a downstream propagated wave. For some values of G^1 the wave has a zero group velocity suggesting again the existence of an absolute instability of the system. The variation of the shear modulus of the middle layer G^2, when $G^1 = G^3 = 0.1$, produces significant variation of the group velocity though the latter remains negative and the wave which is formed by this mode remains an upstream propagated one. The variation of the shear modulus G^3 of the third layer when $G^1 = G^2 = 0.1$, produces a relatively small variation of the group velocity.

The speed of the waves that are propagated in the arteries is a measurable quantity, so the obtained results may be used in order to give insight on the state of the blood vessel and the circulatory system. One has to invert the relation between the group velocity and the shear modulus. In such a way when the speed of the wave is estimated from the measurements one can evaluate the shear modulus of the artery.

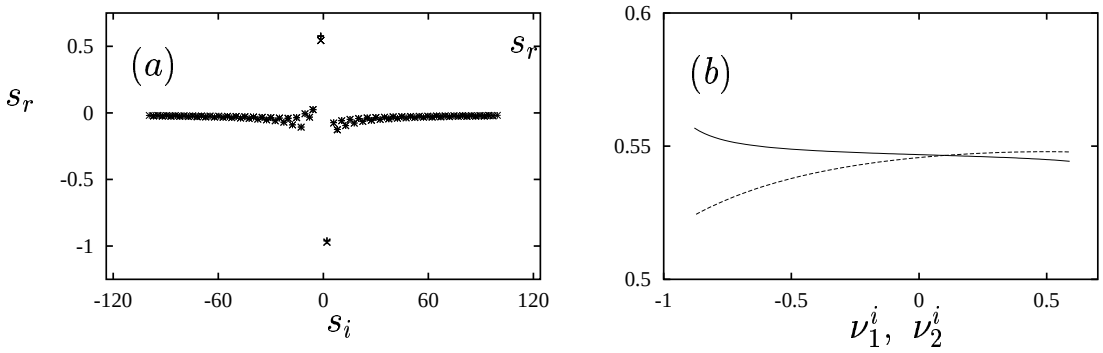

FIG. 2 – (a) : Temporal eigenvalues of three layered viscoelastic tube in the (s_r, s_i)-plane. s_r and s_i being the amplification rate and the frequency, $G^i = 0.1$, $\nu_r^i = 0$, $+$: $\Xi_2^i = 2G^i$, $\Xi_1^i = 20G^i$, $\times$: $\Xi_2^i = 20G^i$, $\Xi_1^i = 2G^i$. (b) : The amplification rate of the most unstable mode versus Poisson coefficients. $\Xi_2^i = 20G^i =$, $\Xi_1^i = 2G^i$. Solid line $\nu_2^1 = \nu_2^2 = \nu_2^2 = 0.1$, $\nu_1^1 = \nu_1^2 = \nu_1^2$ and dashed line $\nu_1^1 = \nu_1^2 = \nu_1^2 = 0.1$, $\nu_2^1 = \nu_2^2 = \nu_2^2$

9 Conclusion

In this paper stability of the compliant biological ducts, like arteries and veins, conveying a viscous fluid has been analyzed. The vessel wall has been modeled as a compliant tube composed of three concentric viscoelastic non-isotropic layers with different material parameters and relative thicknesses. The anisotropy of the layers is connected with differences of the Young's modulus in the radial and axial directions.

The equilibrium state considered here is the steady Poiseuille flow of the viscous incompressible fluid through the hollow cylinder with a constant thickness and inner radius. The length of the cylinder L and its inner radius $R << L$ so it can be considered as an infinitely long tube.

Stability of the system to axisymmetric infinitesimal disturbances has been investigated within the framework of the linear stability analysis. Both temporal and spatial stability analysis have been done and the temporal and spatial eigenvalues of the system have been found. It is shown that anisotropy of the viscoelastic wall has a great effect on stability of the system. For the isotropic tube, it has been found that the temporal eigenvalues form five branches in the (s_r, s_i)-plane where s_r is the amplification rate and s_i is the frequency. Two branches are localized near the positive imaginary axis of the (s_r, s_i)-plane and two others are localized near the

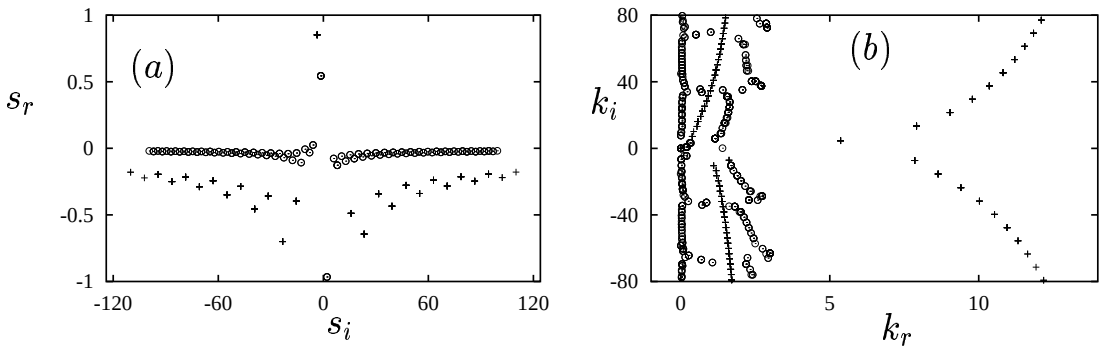

FIG. 3 – Comparison between isotropic and non-isotropic eigenvalues. + : isotropic layers $G^i = 1$, $\Xi^i = 2G^i$. $\odot$: non-isotropic layers, $G^i = 0.1$, $\nu_1^i = \nu_2^i = 0.1$, $\Xi_2^i = 2G^i$, $\Xi_1^i = 20G^i$. (a) : Temporal eigenvalues of three layered viscoelastic tube in the (s_r, s_i)-plane, (b) : Spatial eigenvalues of three layered viscoelastic tube in the (k_r, k_i)-plane

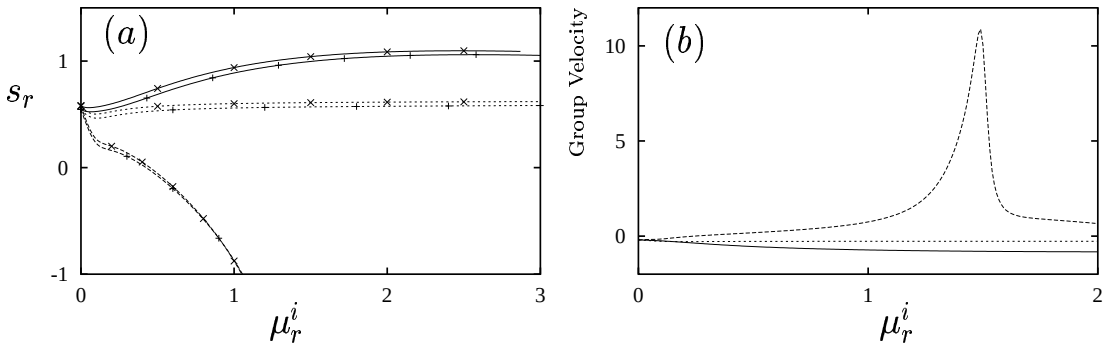

FIG. 4 – (a) : Temporal amplification rate of the most unstable mode versus the viscosity of the three non-isotropic layers. The parameters of the system are $\nu_2^i = \nu_1^i = 0.1$. Solid line $\mu_r^2 = \mu_r^3 = 0$. Dashed line $\mu_r^1 = \mu_r^3 = 0$. Dotted line $\mu_r^1 = \mu_r^2 = 0$. + : $\Xi_2^i = 2G^i$, $\Xi_1^i = 20G^i$, $\times$: $\Xi_1^i = 2G^i$, $\Xi_2^i = 20G^i$. (b) : Group velocity of the most unstable mode versus the viscosity of the three non-isotropic layers. $\nu_1^i = \nu_2^i = 0.1$, $\Xi_2^i = 2G^i$, $\Xi_1^i = 20G^i$. Solid line $\mu_r^2 = \mu_r^3 = 0$. Dashed line $\mu_r^1 = \mu_r^3 = 0$. Dotted line $\mu_r^1 = \mu_r^2 = 0$.

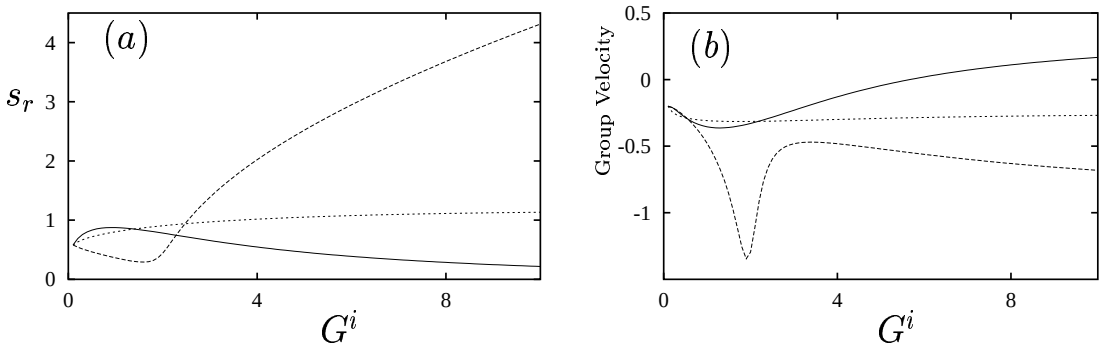

FIG. 5 – (a) : The amplification rate of the most unstable mode versus the shear modulus of the three non-isotropic layers. $\Xi_2^i = 2G^i$, $\Xi_1^i = 20G^i$. Solid line $G^2 = G^3 = 0.1$. Dashed line $G^1 = G^3 = 0.1$. Dotted line $G^1 = G^2 = 0.1$. (b) : Group velocity of the most unstable mode versus the shear modulus of the three non-isotropic layers. $\Xi_2^i = 2G^i$, $\Xi_1^i = 20G^i$. Solid line $G^2 = G^3 = 0.1$. Dashed line $G^1 = G^3 = 0.1$. Dotted line $G^1 = G^2 = 0.1$.

negative imaginary axis and the last one is localized near the real axis. Displacement of the eigenvalues in the (s_r, s_i)-plane can be easily understood by analysis of the eigenvalues of the uncoupled system of equations for the fluid and the solid media. In fact at very low Reynolds numbers, the inertia forces in the fluid are small in comparison with the viscous forces, consequently, the fluid obeys the Stokes equation. Owing the fact that Stokes equation is linear, the disturbance obeys the same Stokes equation. If the disturbance is supposed to be in normal form and the no-slip condition is applied at the interface, then the amplification rate and the frequency, namely s, have to satisfy the following equation

$$s = -\frac{1}{Re} < \frac{\partial v_i}{\partial x_j}, \frac{\partial v_i}{\partial x_j} > / < v_i, v_i >$$

where v_i are the velocity components and the symbol $<,>$ stands for dot product. In this limit case s is real and negative. As expected, at low Reynolds number the modes in the fluid could only be dampened when the no-slip conditions are applied at the solid/fluid interface. Therefore, the modes which are localized near the real axis, when the interaction between the fluid and the solid is allowed, are coming from the fluid into the solid medium. In the same way, if the no-displacement conditions are applied at the solid/fluid interface the eigenvalues of the solid system uncoupled from the fluid have to satisfy the relation

$$s^2 = -G < \frac{\partial u_i}{\partial x_j}, \frac{\partial u_i}{\partial x_j} > / < u_i, u_i >$$

where u_i are the displacement components. In this limit case, the eigenvalues of the solid system are a set of pure positive and negative imaginary numbers. Therefore, the eigenvalues which are localized near the imaginary axis, when the interaction between the fluid and the solid is allowed, are coming from the solid media. When the interaction is allowed between the solid and the fluid at low Reynolds numbers, the eigenvalues are removed slightly from their respective axis to form five branches. As at zero Reynolds numbers the frequency of the fluid modes is zero, by continuity, one expects that at low Reynolds numbers the fluid modes have low frequencies. These fluid low frequency modes are expected to interact more efficiently with the solid modes which have frequencies of the same order of magnitude. The result explains the fact that when the solid/fluid interaction is allowed, the solid modes with low frequencies are moved away from the imaginary axis as it is shown in figure 3. Even though the most important part of the modes are moved by solid/fluid interaction toward the region where $s_r < 0$ producing the stable modes, few of them (in our case two modes) are moved by solid/fluid interaction toward the region where $s_r > 0$ producing two unstable modes.

It has been found that the spatial eigenvalues form four branches in the half-plane $(0 \leq k_r, k_i)$. The similar four branches exist in the half-plane $(0 \geq k_r, k_i)$. Two of the branches represent relatively short waves and two other branches represent relatively long waves. The fact that k_i may be a positive or negative number does not indicate the instability of the system. Rather it indicates the position of the disturbance relative to the source which it has been produced by. In order to find out the values of k_i which are relevant in the spatial instability analysis, one has to lower the Laplace contour of the unstable mode in order to collect the modes which cross the real axis. Thus, these modes represent a spatial instability and the values reached by k_i, when the amplification rate reaches zero, may be interpreted as spatial amplification rates.

It was obtained that an increase in Young's modulus in all the layers with the same rates in the radial or axial directions produces approximately the same effect on the spatial and temporal eigenvalues. Furthermore, the extra diagonal components of linear elasticity tensor have minor effect on the amplification rate of the most unstable mode. We speculate that these extra diagonal components may be more important in the behavior of the asymmetric modes. The stability analysis of these asymmetric modes will be presented soon.

It was found that any increase in the viscosity μ_r^1 of the inner layer while the viscosities of the two other layers are kept constant $\mu_r^2 = \mu_r^3 = 0$, leads to an increase in the amplification rate of the most unstable mode. This result has been explained

by the fact that an increase in the viscosity of the first layer enhance the fluid/solid interaction. Furthermore, it has been found that the viscosity of the middle layer has a stabilizing effect while an increase of the viscosity of the outer layer induces negligible variation of the amplification rate of the most unstable mode (figure 4a).

The difference between the amplification rates of the most unstable mode in the two cases, where in the first case $\Xi_1^j = 2G^j$, $\Xi_2^j = 20G^j$ and in the second case $\Xi_2^j = 2G^j$, $\Xi_1^j = 20G^j$, remains very small for all the viscosity values taken into account. It has been found that the group velocity of the most unstable mode remains negative when the viscosity varies as far as the system is being kept unstable producing an upstream propagated wave. The stability of the system, when μ_r^2 increases, is accompanied by a brutal increase in the wave speed as well as by the variation in its direction (figure 4b).

The dependence of the amplification rate of the most unstable mode on the shear modulus of each layer has been examined. It has been found that an increase in the shear modulus subjected to the relations $\Xi_2^j = 2G^j$ and $\Xi_1^j = 20G^j$, keeps the system unstable. However, the effect of the shear modulus of each layer on the amplification rate has been found to be different. Thus the shear modulus G^1 and G^2 have quasi opposite while G^3 has a relatively small influence on the system (figure 5a). The variation of shear modulus G^1 of the inner solid layer which is in contact with the fluid has been found to exert a great imfluence on the group velocity of the most unstable mode. For the high values G^1 the wave change its direction and becomes a downstream propagated wave.

For some values G^1 the group velocity is zero, which suggests the existence of an absolute instability of the system. The shear modulus of the middle layer G^2 has a noticeable influence on the amplitude of the group velocity of the most unstable mode without changing its direction.

The obtained results confirm that multi-layered structure and mechanical properties of the layers significantly influence flow stability in the compliant tubes. Variations of the elastic and viscous parameters of one of the layer or a few layers simultaneously exert a great influence on the stable and unstable modes. In that way possible stabilizing (destabilizing) effect of the adaptive variations of the parameters of different layers of the blood vessels can be analyzed. The presented results can shed a new light on the mechanics of the arterial wall and its role in stability (instability) of the blood flow in normal and pathological cases. The set of the material parameters which stabilize the liquid flow in the compliant tube can be used in the technical applications for development of the novel stable multi-layered coating and conduits.

Références

[1] Shapiro, A. H., 1977, "Steady Flow in Collapsible Tubes," J. Biomech. Eng., 99(8), pp.126–147.

[2] Kumaran, V., 1998, "Stability of Wall Modes in a Flexible Tube," J. Fluid Mech., 362(5), pp.1–15.

[3] Shankar, V., and Kumaran, V., 2001, "Asymptotic analysis of wall modes in a flexible tube revisited," Europ.Phys.J., Ser.B., 19(4), pp.607–622.

[4] Hamadiche, M., and Gad-el-Hak, M., 2002, "Temporal Stability of Flow Through Viscoelastic Tubes," J. Fluids Structures, 16(3), pp.331–359.

[5] Hamadiche, M., and Gad-el-Hak, M., 2004, "Spatiotemporal stability of flow through collapsible, viscoelastic tubes," AIAA J., 42(4), pp.772–786.

[6] Pedrizzetti, G., 1998, "Fluid Flow in a Tube with an Elastic Membrane Insertion," J. Fluid Mech., 375(11), pp.39–64.

[7] Fung, Y.C., 1990, Biomechanics. Motion, Flow, Stress and Growth, Springer-Verlag, New York.

[8] Humphrey, J. D., 1995, "Mechanics of the Arterial Wall : Review and Directions," Crit. Rev. Biomed. Eng., 23, pp.1–162.

[9] Holzapfel, G.A., Gasser, Th.C., and Ogden, R.W., 2004, "Comparison of a Multi-Layer Structural Model for Arterial Walls With a Fung-Type Model, and Issues of Material Stability," Transactions ASME, 126(4), pp.264–275

[10] Fung, Y.C., and Liu, S.Q., 1995, "Determination of the mechanical properties of the different layers of blood vessels in vivo," Proc.Nat.Acad.Sci. USA, 92(6), pp.2169–2173.

[11] Weber, R., Stergiopulos, N., Brunner, H.R., and Hayoz, D., 1996, "Contributions of Vascular Tone and Structure to Elastic Properties of a Medium-Sized Artery," Hypertension, 27(3), pp.816–822.

[12] Rodriguez-Macias, K.A., Naessen, T., and Bergqvist, D., 2001, "Validation of in vivo noninvasive high-frequency ultrasonography of the arterial wall layers," Ultrasound Med.Biol., 27(6), pp.751–756.

[13] Fischer, E.I.C., Armentano, R.L., Pessana, F.M., et al, 2002, "Endothelium-dependent arterial wall tone elasticity modulated by blood viscosity," Amer.J.Physiol., 282(2), pp.H389–H394.

[14] Gradus-Pizlo, I., Bigelow, B., Mahomed, Y., et al, 2003, "Left anterior descending coronary artery wall thickness measured by high-frequency transthoracic and epicardial echocardiography includes adventitia," Amer.J. Cardiol., 91(1), pp.27–32.

[15] Govyrin, V.A., Didenko, A.V., and Iazykov, V.V., 1998, "Changes in the volume of blood vessel wall in the contractile process," Dokl.Akad.Nauk SSSR, 300(3), pp.745–747.

[16] Johnson, M., and Tarbell, J.M., 2001, "A Biphasic, Anisotropic Model of the Aortic Wall," Transactions ASME, 123(2), pp.52–57.

[17] Vito, R.P., and Dixon, S.A., 2003, "Blood vessel constitutive models - 1995–2002," Annu.Rev.Biomed.Eng., 5, pp.413–439.

[18] Deng, S.X., Tomioka, J., Debes, J.C., and Fung, Y.C., 1994, "New experiments on shear modulus of elasticity of arteries," Amer.J.Physiol., 266(1, Pt 2), pp.H1–H10.

[19] Lu, X., Yang, J., Zhao, J.B., et al, 2003, "Shear modulus of porcine coronary artery :contributions of media and adventitia," Amer. J. Physiol., 285(???), pp.H1966–H1975.

[20] Silver, F.H., Christiansen, D.L., and Buntin, C.M., 1989, "Mechanical properties of the aorta : a review," Crit.Rev.Biomed.Eng., 17(4), pp.323–358.

[21] Debes, J.C., and Fung, Y.C., 1995, "Biaxial mechanics of excised canine pulmonary arteries," Amer.J.Physiol., 269(2), pp.H433–H442.

[22] Zhou, J., and Fung, Y. C., 1997, "The degree of nonlinearity and anisotropy of blood vessel elasticity," Proc.Nat.Acad.Sci.USA, 94(12), pp.14255–14260.

[23] Tozzi, P., Hayoz, D., Oedman, C., et al, 2001, "Systolic axial artery length reduction : an overlooked phenomenon in vivo," Amer.J.Physiol., 280(5), pp.H2300–H2305

[24] Coulson, R.J., Cipolla, M.J., Vitullo, L., and Chesler, N.C., 2004, "Mechanical Properties of Rat Middle Cerebral Arteries With and Without Myogenic Tone," Transactions ASME, 126(2), pp.76–81.

[25] Whale, M.D., Grodzinsky, A.J., and Johnson, M., 1996, "The effect of aging and pressure on the specific hydraulic conductivity of the aortic wall," Biorheology, 33(1), pp.17–44.

[26] Huang, W., and Yen, R.T., 1998, "Zero-stress states of human pulmonary arteries and veins," J.Appl.Physiol., 85(9), pp.867–873.

[27] Stergiopulos, N., Pannatier, A., Rachev, A., Greenwald, S.E.,and Meister, J.-J., 2001, "Assessment of Mechanical Homogeneity of the Arterial Wall by an Artery-Inversion Test," Cardiovasc.Eng., 1(1), pp.31–37.

[28] Qilian, Yu, Zhou, J., and Fung, Y.C., 1993, "Neutral axis location in bending and Young's modulus of different layers of arterial wall," Amer.J.Physiol., 265(1), pp.H52–H60.

[29] Rachev, A., and Hayashi, K., 1999, "Theoretical study of the effects of vascular smooth muscle contraction on strain and stress distributions in arteries," Ann.Biomed.Eng., 27, pp.459–468.

[30] Peterson, S.J., and Okamoto, R.J., 2000, "Effect of residual stress and heterogeneity on circumferential stress in the arterial wall," Transactions ASME, 122(8), pp,454–456.

[31] VanBavel, E., Siersma, P., and Spaan, J.A., 2003, "Elasticity of passive blood vessels : a new concept," Am.J.Physiol., 285(5), pp.H1986–H2000.

[32] Benjamin, T.B., 1963, "The threefold classification of unstable disturbances in flexible surfaces bounding inviscid flows," J.Fluid Mech., 16, pp.436–450.

[33] Carpenter, P.W., and Garrad, A.D., 1985, "The hydrodynamic stability of flow over Kramer-type compliant surfaces. Part 1. Tollmien-Schlichting instabilities," J.Fluid Mech., 155, pp.465–510.

[34] Carpenter, P.W., and Garrad, A.D., 1986, "The hydrodynamic stability of flows over Kramer-type compliant surfaces. Part 2. Flow-induced surface instabilities," J.Fluid Mech., 170, pp.199–232.